Optimizing Sol−Gel Infiltration and Processing Methods for the Fabrication of High-Quality Planar Titania Inverse Opals

Jeremy W. Galusha,[†,§] Chia-Kuang Tsung,[‡,§] Galen D. Stucky,[‡] and Michael H. Bartl*,[†]

Department of Chemistry, University of Utah, Salt Lake City, Utah 84112, and Department of Chemistry and Biochemistry, University of California at Santa Barbara, Santa Barbara, California 93106

Received January 8, 2008. Revised Manuscript Received March 18, 2008

We developed a simple sol−gel chemistry-based opal infiltration method for the fabrication of high-quality planar titania photonic crystals. Polystyrene synthetic opals were infiltrated with a hydrophobic and air/moisture-stable liquid titania precursor. The high stability and hydrophobicity of the titania precursor enabled a new "lift-off/turn-over" backfilling technique that after calcination gives planar titania inverse opals with a flat and completely open surface, without the need for additional processing steps to remove any excess surface coating of the backfilling material. We also compare two different infiltration strategies and their influence on the structural and photonic properties. The obtained inverse opals display excellent photonic properties as evidenced by the presence of first-, second-, and third-order Bragg reflection peaks in accordance with theoretical photonic band structure calculations.

I. Introduction

Photonic crystals, originally proposed by John[1] and Yablonovich[2] in 1987, are an emerging new type of optical material with the potential to manipulate light in nontraditional ways based on photonic band structure concepts.[1–5] The defining characteristic of photonic crystals is a periodic variation of the dielectric function with periodicities on the order of the wavelength of light. Of special interest are three-dimensional (3-D) photonic crystals with the ability to control photon flow in all three spatial dimensions. Inverse opals, a face-centered-cubic air-sphere lattice in a high-dielectric material, are an attractive example of a 3-D photonic crystal,[6–13] because they can be readily synthesized by infiltrating a high-dielectric compound into a sacrificial silica or polystyrene opal template, fabricated by colloidal microsphere self-assembly.[14,15] Two of the most widely used infiltration techniques are sol−gel chemistry for the fabrication of oxide-based inverse opal photonic crystals operating in the visible[8,9,12] and chemical vapor deposition (CVD) for fabricating silicon and germanium photonic crystals operating in the infrared region.[6,10,11,13] While sol−gel chemistry methods are very attractive for their simplicity and ease of fabrication, they often lack the quality and precision of their counterparts created by CVD when the latter is combined with postinfiltration processing steps such as reactive ion etching and/or focused ion-beam milling. Here, we report a new sol−gel chemistry-based infiltration technique that results in the formation of planar titania inverse opal photonic crystals with controlled thickness and a uniformly flat and open surface without the need of postinfiltration structural etching/milling steps. Moreover, we discuss two different infiltration strategies that drastically affect the structural and optical qualities of the sol−gel prepared titania inverse opals.

A central key of our infiltration technique is the modification of the titania sol−gel precursor solution to optimize its infiltration, condensation, and processing properties. Commonly, titanium-alkoxides are directly used as precursors for infiltrating the synthetic opal structures.[8,12] However, titanium-alkoxides are generally air/moisture sensitive and hence make it difficult to control the degree of infiltration, because premature condensation and cross-linking of the precursor clogs the voids of the opal structure at the surface. The anisotropic distribution of titania within these structures as well as surface inhomogeneities make it exceedingly difficult to predict and interpret the optical response.[8,16,17] Various strategies have been employed to overcome this limitation

* Corresponding author. E-mail: bartl@chem.utah.edu.
† University of Utah.
‡ University of California at Santa Barbara.
§ These authors contributed equally to this work.

(1) John, S. *Phys. Rev. Lett.* **1987**, *58*, 2486–2489.
(2) Yablonovitch, E. *Phys. Rev. Lett.* **1987**, *58*, 2059–2062.
(3) Joannopoulos, J. D.; Villeneuve, P. R.; Fan, S. H. *Nature* **1997**, *386*, 143–149.
(4) Lopez, C. *Adv. Mater.* **2003**, *15*, 1679–1704.
(5) Soukoulis, C. M., Ed. *Photonic Crystals and Light Localization*; Kluwer: Dordrecht, 2001.
(6) Blanco, A.; Chomski, E.; Grabtchak, S.; Ibisate, M.; John, S.; Leonard, S. W.; Lopez, C.; Meseguer, F.; Miguez, H.; Mondia, J. P.; Ozin, G. A.; Toader, O.; van Driel, H. M. *Nature* **2000**, *405*, 437–440.
(7) Braun, P. V.; Wiltzius, P. *Nature* **1999**, *402*, 603–604.
(8) Holland, B. T.; Blanford, C. F.; Stein, A. *Science* **1998**, *281*, 538–540.
(9) Subramanian, G.; Manoharan, V. N.; Thorne, J. D.; Pine, D. J. *Adv. Mater.* **1999**, *11*, 1261–1265.
(10) Tetreault, N.; Miguez, H.; Ozin, G. A. *Adv. Mater.* **2004**, *16*, 1471–1476.
(11) Vlasov, Y. A.; Bo, X. Z.; Sturm, J. C.; Norris, D. J. *Nature* **2001**, *414*, 289–293.
(12) Wijnhoven, J.; Vos, W. L. *Science* **1998**, *281*, 802–804.
(13) Miguez, H.; Chomski, E.; Garcia-Santamaria, F.; Ibisate, M.; John, S.; Lopez, C.; Meseguer, F.; Mondia, J. P.; Ozin, G. A.; Toader, O.; van Driel, H. M. *Adv. Mater.* **2001**, *13*, 1634–1637.
(14) Norris, D. J.; Arlinghaus, E. G.; Meng, L.; Heiny, R.; Scriven, L. E. *Adv. Mater.* **2004**, *16*, 1393–1399.
(15) Shimmin, R. G.; DiMauro, A. J.; Braun, P. V. *Langmuir* **2006**, *22*, 6507–6513.
(16) Dong, W. T.; Bongard, H. J.; Marlow, F. *Chem. Mater.* **2003**, *15*, 568–574.

10.1021/cm800072j CCC: $40.75
Published on Web 07/12/2008

such as diluting the precursor solution in ethanol to lower the viscosity and improve the wetting properties of the sol. However, multiple infiltrations are typically required to achieve a mechanically robust final structure.[18–20] An elegant method developed by Pine et al.[21] in which emulsion templating utilizing surfactant stabilized oil in a titania sol is used avoids the infiltration difficulties altogether; however, the polydispersity of the air voids in these samples is twice that found in commonly available polystyrene microspheres.

In contrast to using such instable titanium-alkoxide solutions directly as precursors for the infiltration process, we first react them with a mixture of fluorinated organic and strong inorganic acids, such as trifluoroacetic acid and hydrochloric acid, respectively, precursors that can also be used to fabricate highly ordered meso-structures and composites.[22–24] Solubilizing titanium-alkoxides in organic/inorganic acid mixtures results in a highly air- and moisture-stable sol−gel precursor solution by significantly slowing down the kinetics of condensation. Under these controlled conditions, solubilized titanium-oxide units together with trifluoroacetic acid molecules form stable building blocks for further cross-linking.[24] In addition, the presence of trifluoroacetic acid results in an increase of the hydrophobic character of the precursor, allowing for a more uniform wetting of the polystyrene template during the infiltration process and greater control over the degree of infiltration throughout the entire structure. Furthermore, only a single infiltration cycle is required to produce homogeneous, robust inverse opals.

The choice of infiltration technique also plays a critical role in the quality of the final structure. Common to various methods such as dip-coating and dropwise infiltration[8] is a bulk titania layer that forms at the surface as a result of excess precursor. The presence of this bulk layer can significantly diminish the optical response of the inverse opal samples due to random scattering. While the thickness of the bulk layer can be somewhat reduced by diluting the precursor solution, the filling fraction of the inverse opal is reduced proportionately, necessitating multiple infiltrations as previously mentioned. In contrast, the infiltration process can be conducted within an enclosed volume that limits the amount of bulk titania that can form around the inverse opal sample. The packing cell configuration developed by Xia et al.[25] is an excellent example of this methodology whereby uniformly flat inverse opal structures can be fabricated, although access to clean room facilities is required. In contrast, a simple coverslip can be affixed on top of the sample and the sol−gel precursor allowed to infiltrate the template via capillary forces between the substrate and coverslip.[26] Using a modified "sandwich" capillary infiltration technique, we have reduced the degree of bulk titania formed to a single template monolayer thickness or less. Furthermore, this technique can be combined with our novel "lift-off/turn-over" strategy that allows us to expose the uniformly flat bottom surface of the sample by using adhesive copper tape to remove the sample from the substrate for the calcination process.

As we will discuss in the following, it is the combination of these factors (stability of the precursor; slowed condensation and cross-linking; hydrophobicity), combined with our optimization of sample processing, that are the key factors for fabricating high-quality planar, open-surface titania inverse opal photonic crystals with negligible amounts of bulk titania.

II. Experimental Section

Opal Preparation. The opal templates were prepared from colloidal suspensions of 330, 430, 500, and 740 nm polystyrene spheres (Duke Scientific: hydrophobic; negatively charged sulfonated surface) on glass slides (12.5 mm × 75 mm × 1 mm) according to previously reported methods.[14,15,27,28] Briefly, glass slides were cleaned for ∼30 min in piranha or chromix solution, rinsed with DI water, followed by rinsing with isopropyl alcohol. The cleaned glass slides were then immersed into a 0.05 vol % colloidal suspension of microspheres for ∼36 h.

Inverse Opal Preparation. The titania sol−gel precursor solution was prepared by adding 2 mL of titanium ethoxide (Aldrich) to a mixture of 1.6 mL of trifluoroacetic acid (99%, Aldrich) and 0.4 mL of hydrochloric acid (12 M, Aldrich) while vigorously stirring. After 20 min, the viscosity of the solution was adjusted by adding ethanol and/or ethylene glycol. The voids of the opal templates were then infiltrated with this precursor solution through capillary forces, using either a dip-coating or a sandwich infiltration procedure. For the dip-coating method, the glass slide with the opal template was vertically immersed into the solution for about 20−30 s and then slowly withdrawn at ∼2 cm/min. The sandwich infiltration method consisted of carefully placing an additional glass slide on top of the opal template surface using double-sided tape placed between the two substrates to adhere the surfaces, ensuring that the opal template was flush with the edge of both slides. The very edge of the sandwich structure was then inserted into the sol, and the space between the glass slides as well as the interstitial opal voids were filled by capillary forces. Before further processing, the infiltrated opal/titania composite was allowed to dry for ∼24 h. After drying, the top substrate was removed, an adhesive copper tape was placed on top of the infiltrated opal/titania composite, and the sample was peeled off the glass substrate (see also Figure 1). The sample was then turned upside-down and calcined in air by raising the temperature slowly (1 °C/min) to 450 °C and keeping it there for 6 h. After calcination, the inverse opals were rinsed with hydrochloric acid, water, and acetone, respectively, to remove copper oxide that was formed from the adhesive tape

(17) Holland, B. T.; Blanford, C. F.; Do, T.; Stein, A. *Chem. Mater.* **1999**, *11*, 795–805.
(18) Lanata, M.; Cherchi, M.; Zappettini, A.; Pietralunga, S. M.; Martinelli, M. *Opt. Mater.* **2001**, *17*, 11–14.
(19) Wijnhoven, J. E. G. J.; Bechger, L.; Vos, W. L. *Chem. Mater.* **2001**, *13*, 4486–4499.
(20) Ni, P. G.; Dong, P.; Cheng, B. Y.; Li, X. Y.; Zhang, D. Z. *Adv. Mater.* **2001**, *13*, 437–441.
(21) Manoharan, V. N.; Imhof, A.; Thorne, J. D.; Pine, D. J. *Adv. Mater.* **2001**, *13*, 447–450.
(22) Bartl, M. H.; Boettcher, S. W.; Frindell, K. L.; Stucky, G. D. *Acc. Chem. Res.* **2005**, *38*, 263–271.
(23) Bartl, M. H.; Boettcher, S. W.; Hu, E. L.; Stucky, G. D. *J. Am. Chem. Soc.* **2004**, *126*, 10826–10827.
(24) Boettcher, S. W.; Bartl, M. H.; Hu, J. G.; Stucky, G. D. *J. Am. Chem. Soc.* **2005**, *127*, 9721–9730.
(25) Zhong, Z. Y.; Yin, Y. D.; Gates, B.; Xia, Y. N. *Adv. Mater.* **2000**, *12*, 206–209.
(26) Zhou, Q.; Dong, P.; Yi, G. Y.; Liu, L. X.; Cheng, B. Y. *Chin. Phys. Lett.* **2005**, *22*, 1155–1158.
(27) Im, S. H.; Kim, M. H.; Park, O. O. *Chem. Mater.* **2003**, *15*, 1797–1802.
(28) Jiang, P.; Bertone, J. F.; Hwang, K. S.; Colvin, V. L. *Chem. Mater.* **1999**, *11*, 2132–2140.

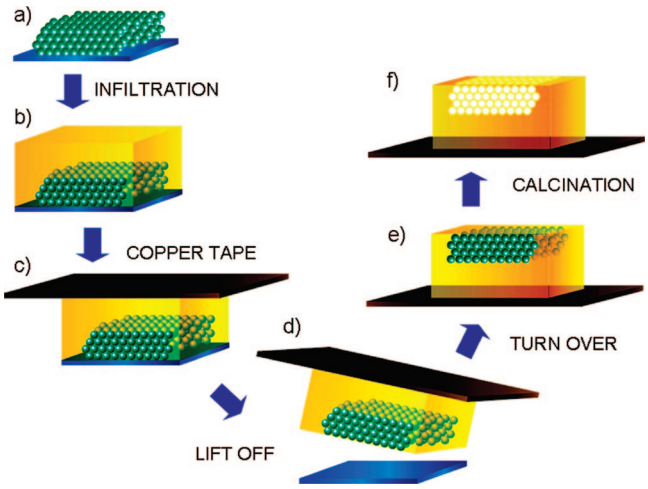

Figure 1. Schematic showing the "lift-off/turn-over" inverse opal fabrication technique. (a) Planar polystyrene opal template. (b) Infiltrated opal/titania sol composite structure. (c) Dried infiltrated opal/titania gel composite structure with adhesive copper tape placed on top. (d) Lift off of the opal/titania composite from the silica substrate. (e) The opal/titania composite structure is turned over so that the flat opal-terminated surface is on top. (f) Calcined titania inverse opal with planar open surface.

during calcination. The cleaned samples were dried at elevated temperatures before structural and optical studies.

Characterization Studies. A modified optical microscope (Nikon ME600) was used for reflectance imaging of the samples. For optical microreflectance spectroscopy measurements, the same microscope was fiber-coupled to a USB UV−vis spectrometer (Ocean Optics), and the reflectance spectra were collected using a 20× objective (0.45 N.A.). A high reflectance broadband mirror ($R > 0.99$) was used as reference. An aperture was inserted into the image plane of the optical path to reduce the probed area to a spot of ~10 μm in diameter. Scanning electron microscopy studies were performed on a Philips XL30 ESEM FEG electron microscope. X-ray diffraction was done on a Philips X'Pert XRD powder diffractometer using Cu Kα radiation.

Theoretical Studies. Band structure calculations were performed using the MIT Photonic-Bands package (MPB).[29] The titania inverse opal model that was used for the calculations consists of close-packed air spheres with radius sqrt(0.5)/2, surrounded by overlapping higher dielectric material ($n = 2.3$; see Supporting Information for details on refractive index determination), with radius 1.09 in units of the air-sphere radius. Each air sphere is connected to its 12 nearest neighbors using cylindrical windows with radius 0.4 in units of the air sphere radius.[30] This geometry results in a filling fraction (*ff*) of 14.5% for the high dielectric component. These model parameters, which gave the best convergence between the experimentally obtained optical data and calculated midgap locations, are in good agreement (within experimental error) of the sample parameters determined by SEM (see also Supporting Information).

III. Results and Discussion

(A) The Lift-Off/Turn-Over Fabrication Technique. The basic fabrication steps of our method, which could be best described as a "lift-off/turn-over" technique, are shown in Figure 1. Planar opal colloidal crystals with controlled thicknesses serve as removable templates for the fabrication of titania inverse opals. These opal templates are then infiltrated with our titania sol−gel precursor by a dip-coating or a sandwich infiltration approach (see below). In both cases, the interstitial sites of the opal template are filled through capillary forces. The increased air/moisture stability as a result of the slowed condensation and cross-linking kinetics of the titanium oxide/trifluoroacetic acid molecular building blocks and the induced hydrophobicity of the titania precursor solution not only enables a very uniform and complete infiltration of the polystyrene opal template, but in addition reduces the adherence of the infiltrated titania−polystyrene opal structure to the underlying hydrophilic silica glass substrate. Consequently, after gelation of the infiltrated titania precursor, the whole structure can easily be removed from the silica substrate. We make use of this property by placing an adhesive substrate on top of the bulk titania layer. This allows us to then peel off the infiltrated opal structure from the bottom substrate so that after turning it upside down a uniformly flat opal-template-terminated surface is exposed. However, it should be noted that the efficacy of the removal process was found to be highly dependent upon the substrate preparation prior to opal growth. In more detail, we found that by including a final rinsing step using isopropanol, almost complete removal of the opal−sol composite could be obtained. Without this step, while we noted no decrease in the hydrophilicity of the substrate as indicated by the opal film quality, only negligible amounts of the composite could be removed. While the exact mechanism behind this observation will be investigated in detail, at this point we speculate that the effect of the isopropanol wash is to reduce the attraction between the positively charged native silica surface and the negatively charged polystyrene microspheres, where the positive charge on silica comes from the acidic nature of the titania sol−gel infiltration solution (pH ≈ 1), which is below the isoelectric point of silica, and the negative charge on polystyrene spheres stems from residual sulfate groups. The last step of the fabrication process is a heat treatment in an oxidative environment to remove the polystyrene opal template and to transform the infiltrated titania precursor into a polycrystalline anatase phase, as confirmed by X-ray diffraction (see Supporting Information). The final structure is a titania inverse opal with a flat and open surface, without the use of additional processing steps such as etching and milling that are in general required to remove this excess bulk layer, and which introduce unwanted photonic surface-defect states.[11]

The structural properties of the fabricated titania photonic crystals are examined by scanning electron microscopy. Results are given in Figure 2 and reveal that our "lift-off/turn over" fabrication technique produces highly ordered inverse opal photonic crystal structures with a planar surface and single crystalline domains of tens of microns (Figure 2c). High-resolution micrographs recorded along the [111] and [100] crystal axes of the face-centered-cubic air-sphere lattice are shown in Figure 2a and b, respectively. These views not only reveal the excellent uniformity of structural details such as wall thickness and interconnecting windows, but also underline the efficiency of the infiltration process. Additionally, because our fabrication method does not require

(29) Johnson, S. G.; Joannopoulos, J. D. *Opt. Express* **2001**, *8*, 173–190.
(30) Vos, W. L.; van Driel, H. M. *Phys. Lett. A* **2000**, *272*, 101–106.

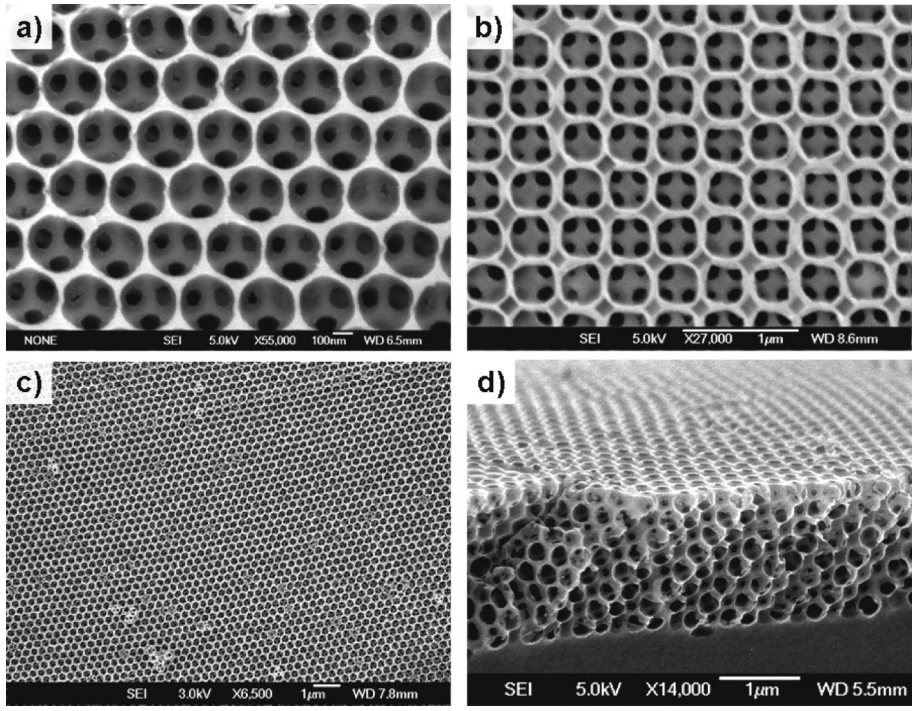

Figure 2. SEM images of planar open-surface titania inverse opal photonic crystals obtained via the sandwich infiltration technique. (a) View along the [111] direction. (b) View along the [100] direction. (c) Large area view along the [111] direction. (d) Side view of the fcc-arranged air-sphere lattice in titania.

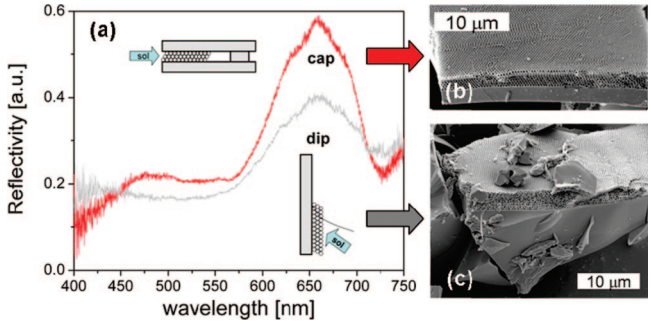

Figure 3. Comparison of titania inverse opal photonic crystals originating from the same opal template, however, prepared differently, sandwich (cap) and dip-coating (dip) infiltration methods. (a) Optical reflectance spectra with insets showing schematics of the two infiltration techniques. (b and c) SEM images of the samples prepared by sandwich infiltration (b) and dip-coating infiltration (c).

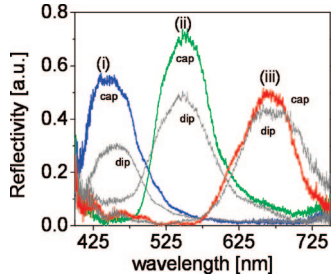

Figure 4. Optical reflectance spectra comparing sandwich (cap) and dip-coating (dip) infiltration methods for titania inverse opals prepared from polystyrene opals with sphere diameters: (i) 330 nm, (ii) 430 nm, and (iii) 500 nm. Data have been baseline corrected for clarity.

any postinfiltration processing steps such as etching or milling, the inverse opal structure has a uniform and predetermined (by the opal template) thickness (Figure 2d), which can be adjusted simply by varying the parameters used for the microsphere deposition process.

(B) Influence of Infiltration Methods on the Photonic Properties. The dip-coating approach naturally results in a bulk titania layer covering the inverse opal structure. While the thickness of the bulk titania layer can be varied by changing solution viscosity and the withdrawal speed of the substrate, it cannot be completely avoided using this technique. A typical sample prepared using this method with a thick bulk titania layer can be seen in Figure 3c. Because of the differences in mechanical properties between the bulk titania layer and the porous titania inverse opal structure, stresses that are introduced during the drying and calcination steps often lead to severe structural distortions such as bending or curling in the final structure. Additionally, the thick bulk layers tend to fracture randomly, resulting in the (111) crystal face lying at highly oblique angles from normal. Such structural deviations from the planar structure have a profound effect on the resulting photonic properties, especially when collecting optical data at normal incidence to the film top surface.

Alternatively, we found that by using a sandwich infiltration procedure the thickness of the bulk layer could be reduced in many cases to less than the thickness of a single monolayer in the inverse opal structure as seen in Figure 3b. The key to this sandwich infiltration method, schematically illustrated in Figure 3a (top inset), consists of the use of a small section of glass slide as a spacer between the sample and top substrates, with double-sided tape used to adhere the pieces together. Initially, we tried sandwiching the opal template between two slides without a spacer; however, this led to significant anisotropic depressions in the crystalline structure due to the sensitivity of the infiltrated polystyrene opal to pressure. By incorporating the spacing material, we found we could eliminate these effects com-

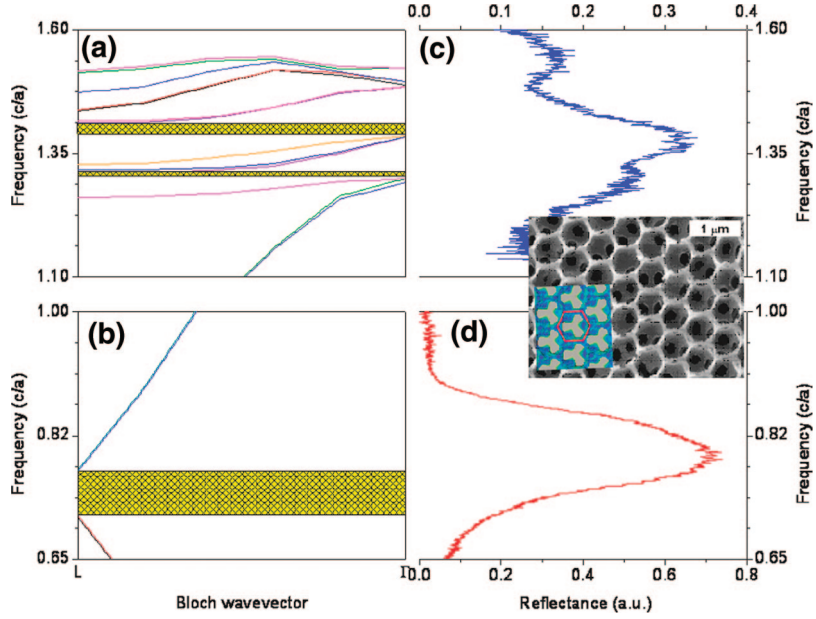

Figure 5. Left side: (a) Calculated high-frequency and (b) low-frequency band structure diagram showing the Γ-L [111] direction for an inverse opal (n = 2.3, ff = 14.5%) made of air spheres surrounded by overlapping higher refractive index, n, shells (radius 1.09 in units of air sphere radius). Stop gaps are indicated by the hatched regions. Right side: Optical reflectance spectra of planar open-surface titania inverse opal photonic crystals with lattice constants of (c) a = 535 nm and (d) a = 310 nm. Data have been baseline corrected for clarity. Inset: SEM micrograph of a titania inverse opal with a lattice constant of a = 535 nm along with the calculated dielectric function (lower left corner).

pletely, resulting in planar inverse opal structures with uniformly thin bulk titania layers underneath.

While SEM analysis reveals the drastic improvement in structural properties using the capillary infiltration method, reflection spectroscopy further illustrates the superiority of this technique (Figure 3a). This is shown in Figure 4, where a series of reflectance spectra collected from titania inverse opals prepared from microspheres of different diameters are compared for the dip-coating and sandwich infiltration methods. To minimize possible differences in inverse opal thickness and defect density, dip-coated and sandwich-infiltrated inverse opal samples for reflectance spectroscopy studies were prepared from the same opal template films. In detail, after opal film growth, the sample was divided and one-half was backfilled with the titania sol−gel compound by dip-coating and the other half by capillary infiltration. Spectra were then taken and compared from different parts of the inverse opals to account for local inhomogeneities (local defects, cracks, etc.). In general, we observed in reflectance spectroscopy studies that regardless of the inverse opal lattice constants the sandwich-infiltrated samples outperformed the dip-coated samples. A representative comparison is shown in Figure 4, where the sandwich-infiltrated samples have a significant higher reflectivity as compared to the dip-coated samples, thus providing further evidence for both the increased uniformity of the surface/sample morphology as well as the elimination of large area structural distortions such as bending.

(C) Calculations and Optical Spectroscopy. Theoretical band structure calculations and optical reflectance spectroscopy were used to characterize the photonic properties of the titania inverse opals in more detail.[29] The left-hand side of Figure 5 shows the calculated photonic band structure in the Γ-L [111] direction for the high- and low-frequency regime (Figure 5a and b, respectively). The calculations reveal that in addition to the first-order low-frequency stop gap (between the second and third bands) two additional higher-frequency stop gaps between the fifth and sixth bands (second-order stop gap) and the eighth and ninth bands (third-order stop gap) are present. To experimentally verify the presence of these stop gaps in our titania photonic crystals, we performed optical reflectance measurements normal to the (111) surface plane (Γ-L direction) of planar inverse opals prepared via the sandwich infiltration method. To examine both the low- and the high-frequency regime, two samples with different lattice constants were prepared, and the obtained spectra were normalized with respect to the respective lattice constants. To verify the correlation of the results of the band structure calculations with the real inverse opal sample used for the spectroscopic measurements, the dielectric function corresponding to the calculated band structure was also evaluated and compared to the SEM images of the actual samples. As an example, the inset of Figure 5 shows such a comparison of the calculated dielectric function and the real SEM image of the inverse opal sample that was used for probing the high frequency regime (with a lattice constant of a = 535 nm).

The results of the optical reflectance spectroscopy measurements are shown on the right side of Figure 5, where the reflectance spectra of the high-frequency regime (Figure 5c) and the low-frequency regime (Figure 5d) were obtained from titania inverse opals with lattice constants of a = 535 nm and a = 310 nm, respectively. A comparison of these spectra with the band structure diagram not only shows the excellent agreement of the spectra with the calculations, but also shows that in our samples the high-frequency stop gaps (second- and third-order gaps) are clearly evident as two reflection peaks. This is of importance, because, in contrast

to the very robust first-order stop gap in inverse opals, the higher-frequency region is very sensitive to structural defects due to the increased density of optical bands. Therefore, small crystal imperfections can readily close these higher-order stop gaps.[30,31] The ability to experimentally detect both the second- and the third-order stop gaps therefore underlines the excellent quality of the titania inverse opal photonic crystals obtained by the combination of our lift-off/turn-over fabrication technique with the sandwich infiltration strategy.

IV. Conclusions

Sol−gel methods present a fast, simple, and relatively inexpensive route toward the preparation of inverse opal photonic crystals, but are a challenge in terms of achieving a high degree of photonic quality. We have shown that the structural and optical qualities depend strongly upon the fabrication parameters, such as sol−gel precursor composition/properties, infiltration technique, and precalcination sample processing. By combining colloidal self-assembly templating with a new titania sol−gel infiltration technique, we have created inverse opals with a flat, completely open surface and uniform thickness without the need of etching or milling steps. The high quality of these inverse opal photonic crystals is expressed by the presence of the high-frequency second- and third-order stop bands in the Γ-L [111] direction, in agreement with theoretical calculations. These excellent photonic properties combined with their precisely defined shape should make these inverse opal structures attractive candidates for emerging applications of photonic crystals operating in the visible wavelength region, such as optically amplified solar energy conversion[32–34] and photocatalysis.[35]

Acknowledgment. This work was supported in part by the National Science Foundation under Award No. ECS 0609244 (M.H.B.) and Award No. DMR 0233728 (G.D.S.), the Utah FIS grant program, and by start-up funds from the University of Utah. M.H.B. acknowledges financial support from the Max Kade Foundation, NY. We would like to thank Prof. Evelyn Hu and Shannon Boettcher for valuable discussions.

Supporting Information Available: Powder X-ray spectrum of titania inverse opal showing that the walls are composed of anatase phase; method of determining the refractive index of the titania framework walls of the inverse opal structure (PDF). This material is available free of charge via the Internet at http://pubs.acs.org.

CM800072J

(31) Li, Z. Y.; Zhang, Z. Q. *Phys. Rev. B* **2000**, *62*, 1516–1519.
(32) Halaoui, L. I.; Abrams, N. M.; Mallouk, T. E. *J. Phys. Chem. B* **2005**, *109*, 6334–6342.
(33) Mihi, A.; Miguez, H. *J. Phys. Chem. B* **2005**, *109*, 15968–15976.
(34) Nishimura, S.; Abrams, N.; Lewis, B. A.; Halaoui, L. I.; Mallouk, T. E.; Benkstein, K. D.; van de Lagemaat, J.; Frank, A. J. *J. Am. Chem. Soc.* **2003**, *125*, 6306–6310.
(35) Chen, J. I. L.; von Freymann, G.; Choi, S. Y.; Kitaev, V.; Ozin, G. A. *Adv. Mater.* **2006**, *18*, 1915–1919.